Supporting Information

Comparative Study of Oxygen Source Doping Effects on the Multidimensional Stability of $Li_{5.5}PS_{4.5}Cl_{1.5}$ Solid Electrolytes

Liang Ming[1, 2, #], Chen Liu[2, #], Siwu Li[1], Ziling Jiang[2], Lin Li[2], Ziyu Lu[2], Qiyue Luo[2], Miao Deng[2], Chuang Yu[1, 2, *]

[1]*School of Information Mechanics and Sensing Engineering, Xidian University, Shanxi 710126, P. R China*

[2] *School of Electrical and Electronic Engineering, Huazhong University of Science and Technology, Wuhan 430074, P. R. China*

[*]Corresponding authors:
E-mail addresses: cyu2020@hust.edu.cn (Chuang Yu)

Experimental

1. Materials synthesis

$Li_{5.5}PS_{4.425}O_{0.075}Cl_{1.5}$ (LPSCO) electrolytes were synthesized via ball milling followed by subsequent heat treatment. Raw materials including Li_2S (Aladdin, 99.98%), P_2S_5 (Aladdin, 99.9%), LiCl (Macklin, 99%), Li_2O (Aladdin, 99%) , P_2O_5 (Aladdin, 99%) were placed into tungsten carbide mill pots with stoichiometric ratio. Each tungsten carbide mill pot contained 2 g of raw materials and 10 the tungsten carbide beads (Φ=10 mm). Ball milling process was performed on Retsch (PM 200) at a rotation speed of 500 rpm for 16 h. The ball milled electrolytes were pelletized into a pellet for annealing. The obtained precursor pellet was sealed into a quartz tube. Finally, the annealing process were conducted under 500 for 6 h. All above process were performed in a Argon glovebox (H_2O＜0.1 ppm, O_2< 0.1 ppm).

2. Preparation of composite cathode

The ZrO_2-coated $LiNi_{0.9}Co_{0.05}Mn_{0.05}O_2$ (ZrO_2@$LiNi_{0.9}Co_{0.05}Mn_{0.05}O_2$)/$Li_{5.5}PS_{4.425}O_{0.075}Cl_{1.5}$ (SSEs after air exposure and heat treatment)/VGCF (Vapor-Grown Carbon Fiber) composite cathode were prepared by milling ZrO_2@$LiNi_{0.9}Co_{0.05}Mn_{0.05}O_2$ cathode active materials, SSEs and VGCF in the mass ratio of 70:28:2 at 110 rpm for 1 h in ZrO_2 pot.

3. Material Characterization

X-ray diffraction (XRD) data of the obtained samples were obtained via a SmartLab-SE Powder instrument using Cu K_α radiation in a range of 10-80°. XRD refinement data were collected by the Rietveld method using GSAS. The morphology

characterization of samples was carried out in a SEM equipment (Nova NanoSEM 450).

4. Air stability measurements

200 mg of solid electrolyte was pressed into the pellet. 30 min after pellets exposure to the atmosphere of 26 °C and 30% humidity, ionic conductivity was measured. After exposure, the exposed samples were heated treated at designated temperatures under vacuum.

5. Electrochemical characterization

Electrochemical impedance spectroscopy (EIS) measurements were performed on an impedance analyzer (Biologic, SP-300) in the frequency of 0.1 -10^7 Hz with a perturbation of 10 mV. The SS/SSEs/SS symmetric cells were assembled with 150 mg SSEs under 380 MPa at room temperature.

6. Fabrication of all-solid-state battery

Assembled ASSBs are composed of composite cathode/ sulfide/Li-In anode. Firstly, 100 mg of $Li_{5.5}PS_{4.425}O_{0.075}Cl_{1.5}$ were dividually put into a PTFE cylinder with diameter of 10 mm under 10 MPa. Afterwards 1 composite cathode was added and pressed on the side of $Li_{5.5}PS_{4.425}O_{0.075}Cl_{1.5}$ electrolytes under 380 MPa. Finally, Li-In alloy was attached to the other side of bilayer electrolytes under 150 MPa. Stack pressure of 70 MPa was used to maintain the sandwiched structure during charge/discharge process. Cathode loading mass in ASSBs are 4.46 mg cm^{-2} The fabrication process were performed in a Argon glovebox (H_2O＜0.1 ppm, O_2< 0.1 ppm) . The charge/discharge test were performed on Neware (CT4008) between 2.4-

3.7 V (vs. Li-In) at various current densities under different temperature (-20 ℃, RT, 60 ℃).

7. Computational details

Density functional theory (DFT) calculations were performed using the Vienna Ab initio Simulation Package (VASP). The Perdew–Burke–Ernzerhof (PBE) functional within the generalized gradient approximation (GGA) was adopted to describe the exchange–correlation interactions, together with the projector augmented wave (PAW) method for treating the electron–ion interactions. A plane-wave cutoff energy of 520 eV was used throughout the calculations. The Brillouin zone integration was carried out using a 3 × 3 × 3 Monkhorst-Pack k-point mesh. Geometry optimizations were conducted with the conjugate-gradient algorithm until the total energy converged to 1 × 10^{-5} eV per atom and the residual atomic forces were below 0.05 eV $Å^{-1}$.

LPSC crystallizes in the cubic space group $F\bar{4}3m$. To identify the most stable structural configuration, the initial candidate models were screened based on the Madelung potential, and the four energetically favorable structures were selected for further geometry optimization. Oxygen substitution was then introduced at the 4c and 16e crystallographic sites to model different doping concentrations. For each doped configuration, both structural optimization and electronic structure calculations were performed. The oxygen doping in LPSC can be introduced through either Li_2O or P_2O_5, and the corresponding reaction pathways are expressed as:

$7\ Li_2S + 2\ P_2S_5 + 6\ LiCl + 1\ Li_2O \rightarrow Li_{22}P_4S_{17}Cl_6O$

$40\ Li_2S + 9\ P_2S_5 + 30\ LiCl + P_2O_5 \rightarrow 5\ Li_{22}P_4S_{17}Cl_6O$

The formation energy of the oxygen-doped LPSC was calculated according to the following expression:

$$E_f(LPSCO) = \frac{\sum \mu_i E(product) - \sum \rho_i E(reactant)}{n(product\ atoms)}$$

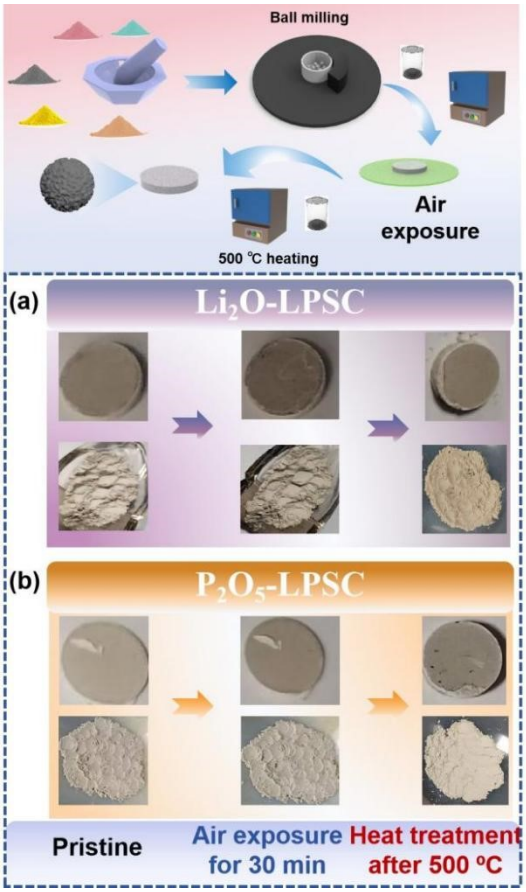

Fig. S1. Digital images of electrolytes in different conditions including pristine, air-exposed, and heat treated. (a) Li_2O-LPSC, (b) P_2O_5-LPSC.

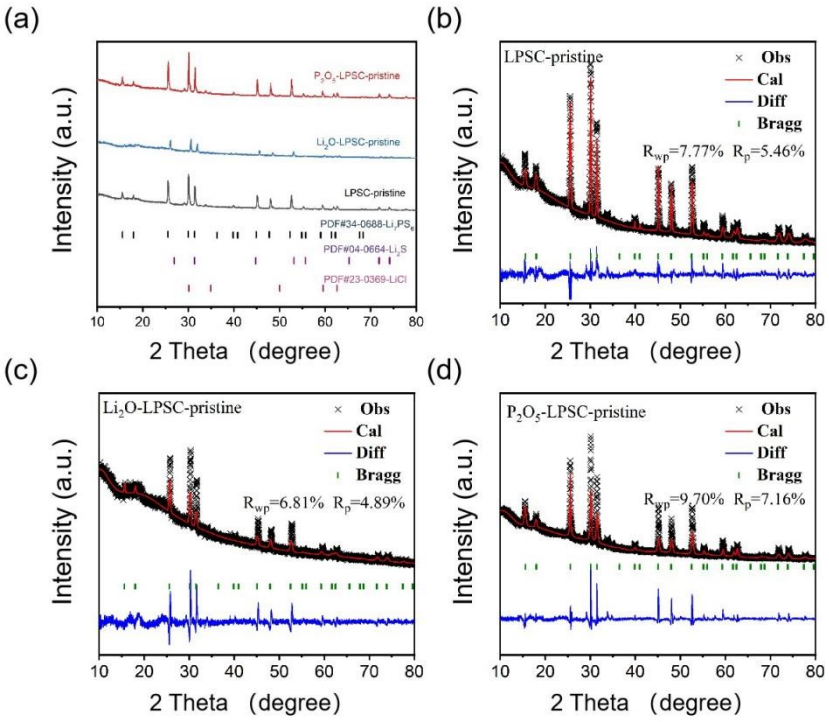

Fig. S2. XRD patterns of pristine LPSC, Li_2O-LPSC, and P_2O_5-LPSC; Corresponding Rietveld refinements patterns of (b) pristine-LPSC, (c) Li_2O-LPSC, and (d) P_2O_5-LPSC.

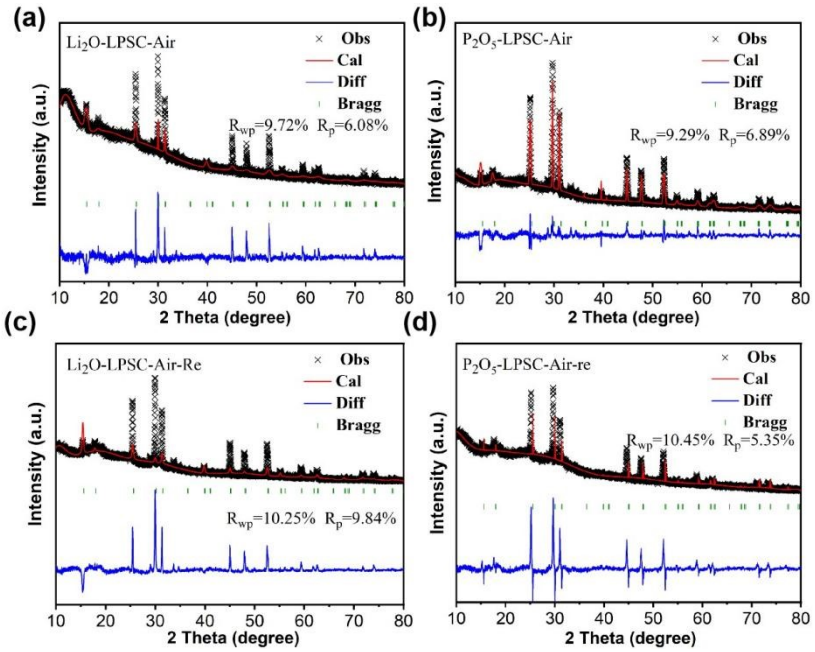

Fig. S3. XRD Rietveld refinements patterns of pellet (a) Li_2O-LPSC-Air, (b) P_2O_5-LPSC-Air, (c) Li_2O-LPSC-Air-Re, and (d) P_2O_5-LPSC-Air-Re.

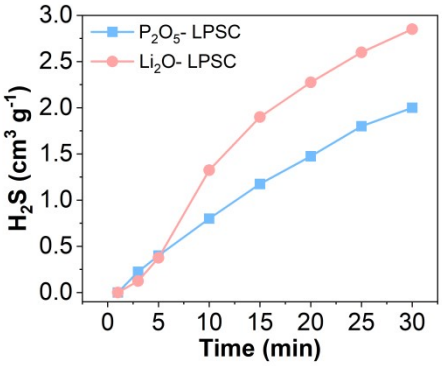

Fig. S4. The generation rates of H_2S released by both SSEs at 30.0% relative humidity and ambient temperature over a duration of 30 minutes.

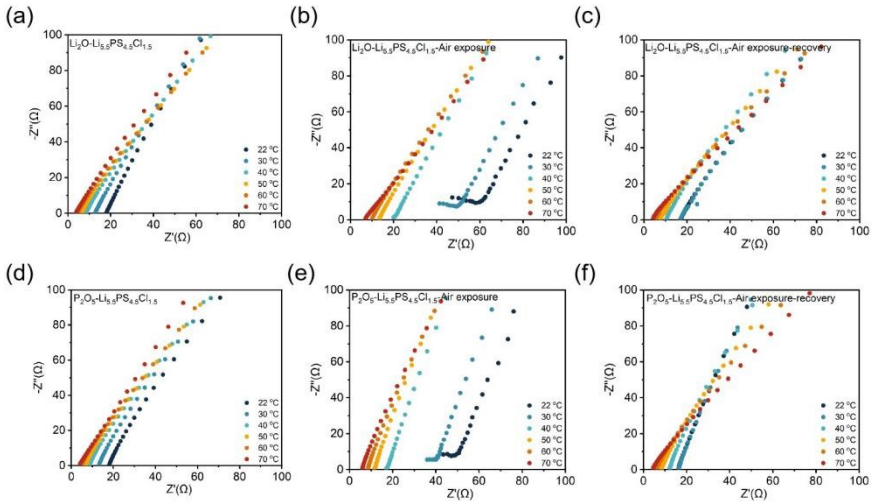

Fig. S5. Nyquist plots of (a) Li_2O-LPSC-pristine, (b) Li_2O-LPSC-Air, (c) Li_2O-LPSC-Air-Re, (d) P_2O_5-LPSC-pristine, (e) P_2O_5-LPSC-Air, (c) P_2O_5-LPSC-Air-Re.

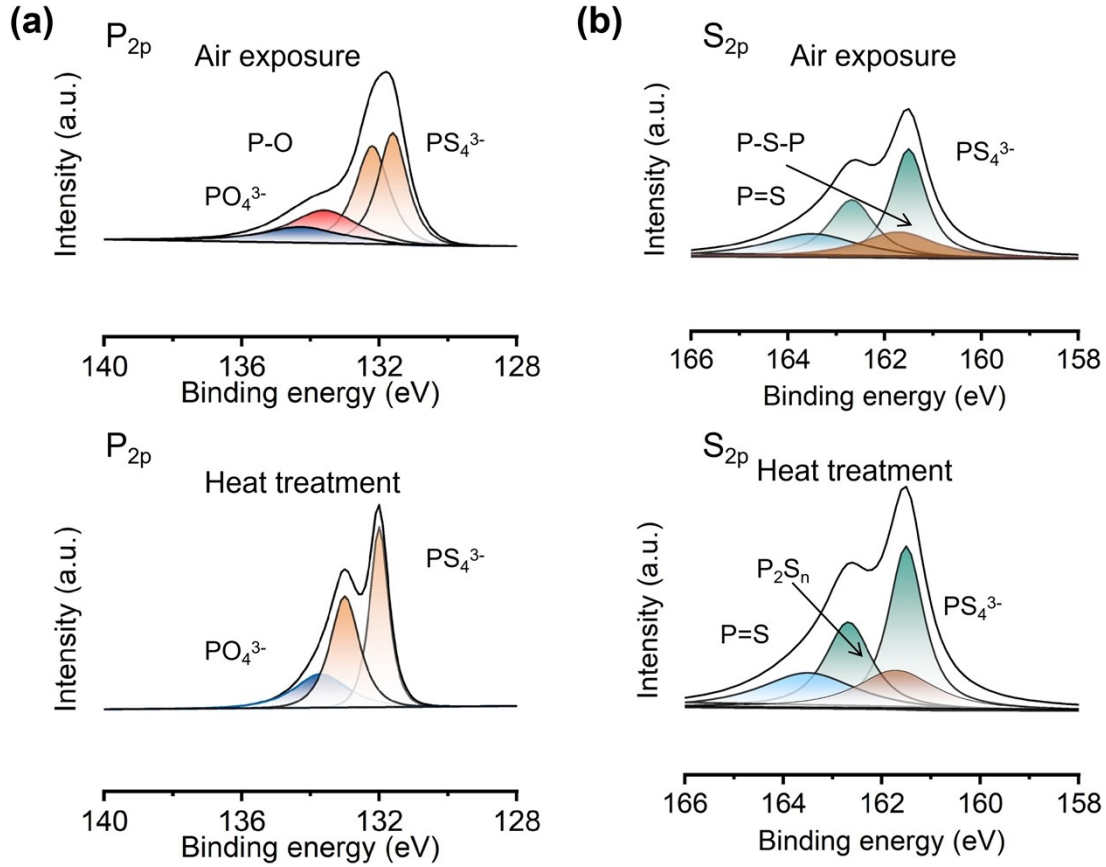

Fig. S6. X-ray photoelectron spectrum of air-exposed and recovered (a)P 2p and (b)S 2p.

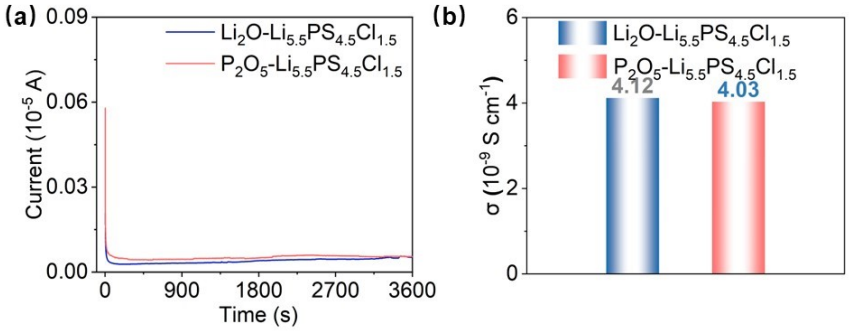

Fig. S7. (a) DC polarization curves for the synthesized Li_2O-LPSC and P_2O_5-LPSC. solid electrolytes. (b) Room-temperature electronic conductivity values of the Li_2O-LPSC and P_2O_5-LPSC electrolytes.

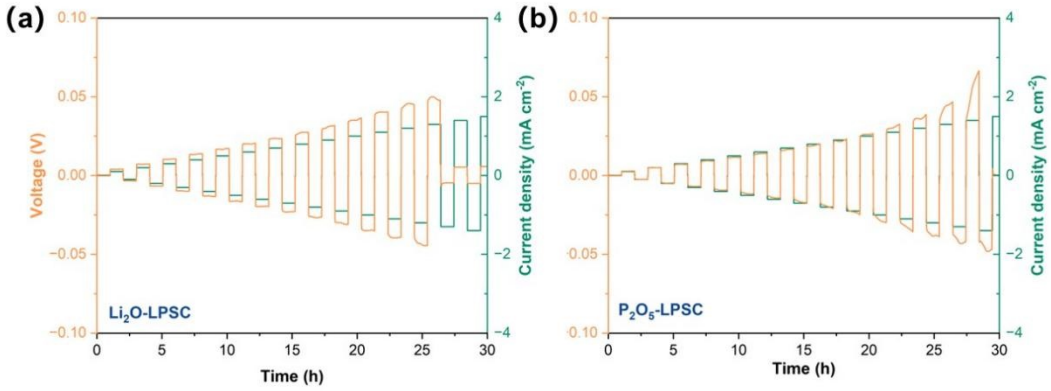

Fig. S8. The CCD measurements for (a) Li/ Li_2O-LPSC /Li, and (b) Li/ P_2O_5-LPSC /Li.

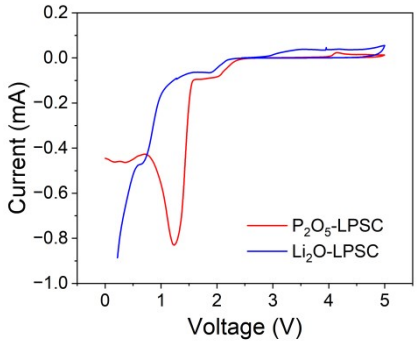

Fig. S9. Cyclic voltammetry plots of the asymmetric Li/ Li_2O-LPSC or P_2O_5-LPSC / Li_2O-LPSC or P_2O_5-LPSC +C cells.

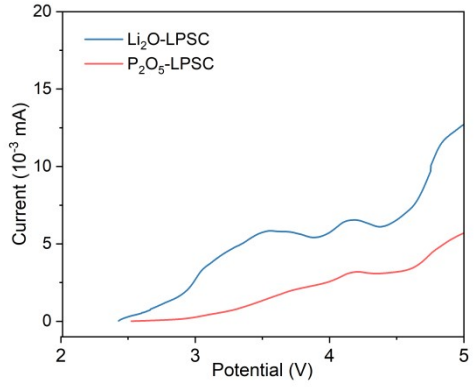

Figure. S10 Linear sweep voltammetry curves of Li_2O-LPSC and P_2O_5-LPSC electrolytes.

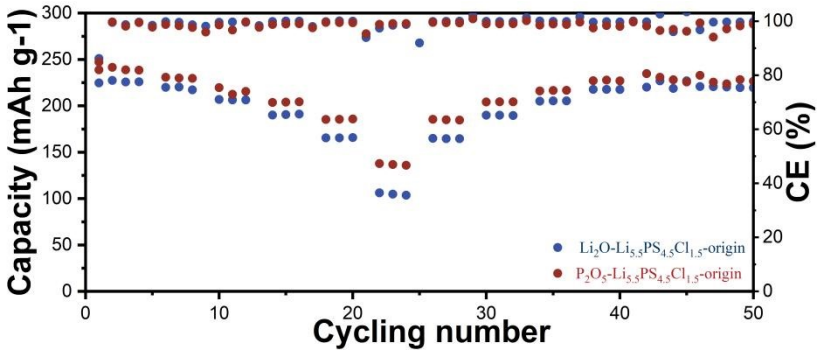

Fig. S11. Rate performance of ASSBs using pristine (a) Li_2O-LPSC, (b) P_2O_5-LPSC.

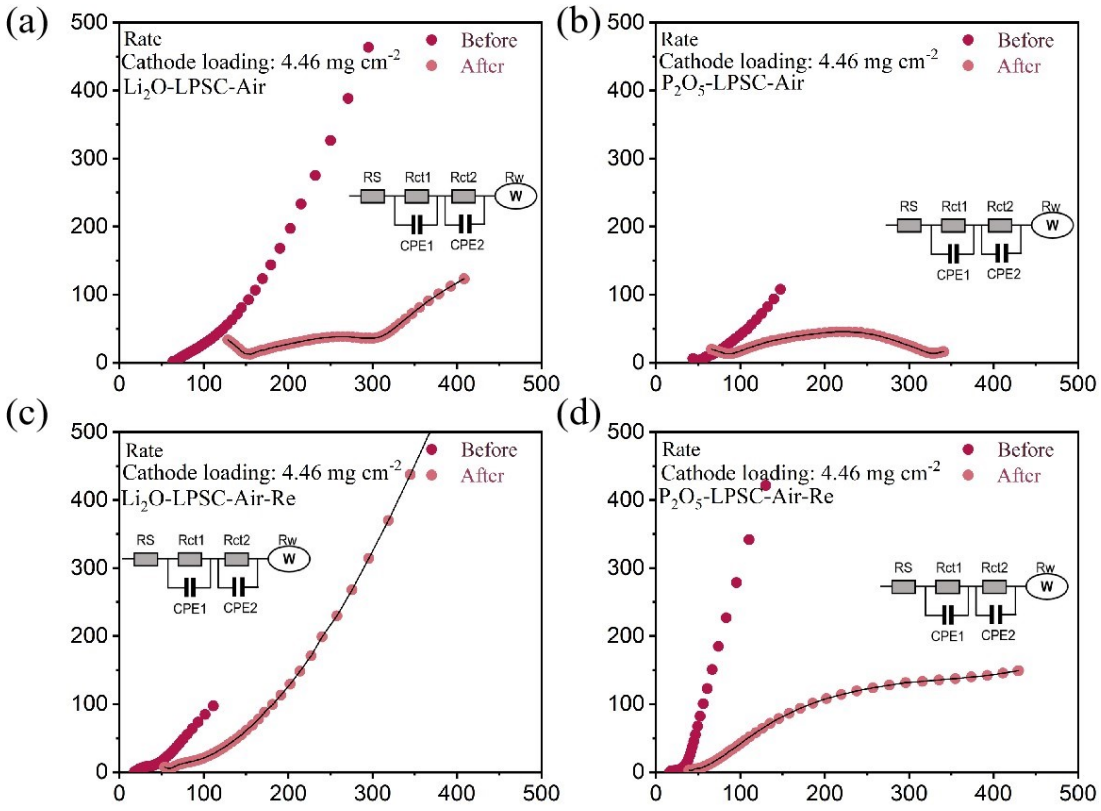

Fig. S12. Impedance spectra of ASSBs using (a) Li_2O-LPSC-Air, (b) P_2O_5-LPSC-Air, (c) Li_2O-LPSC-Air-Re and (d) P_2O_5-LPSC-Air-Re after rate tests.

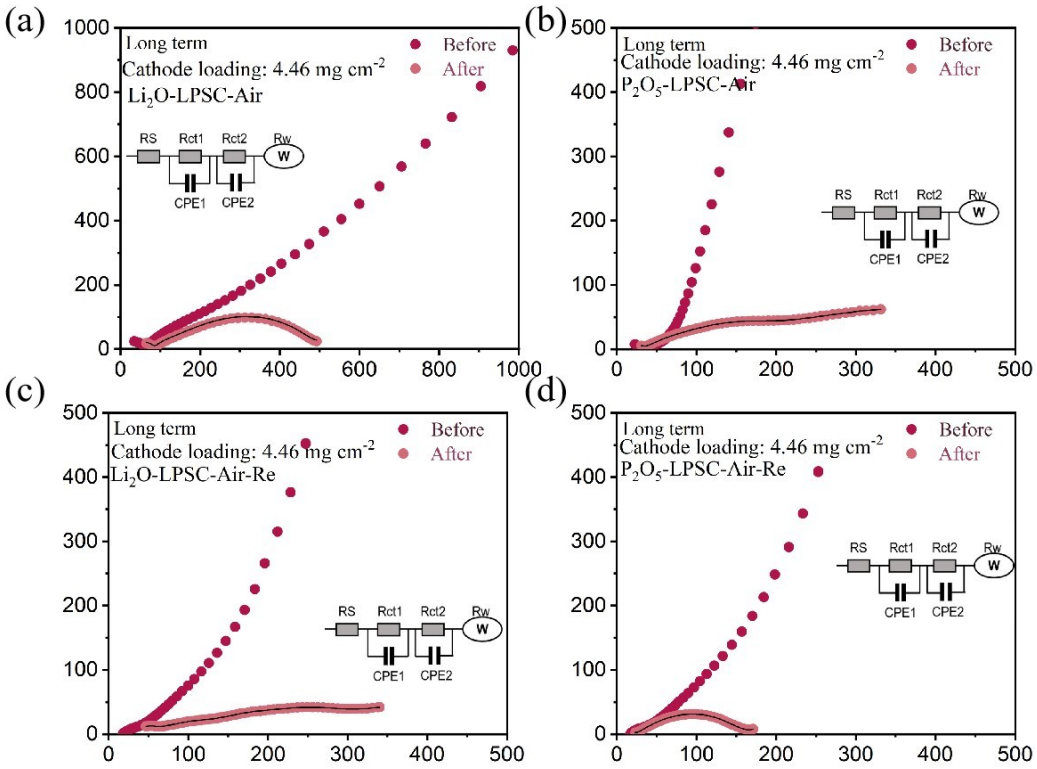

Fig. S13. Impedance spectra of ASSBs using (a) Li_2O-LPSC-Air, (b) P_2O_5-LPSC-Air, (c) Li_2O-LPSC-Air-Re and (d) P_2O_5-LPSC-Air-Re after long-term cycling.

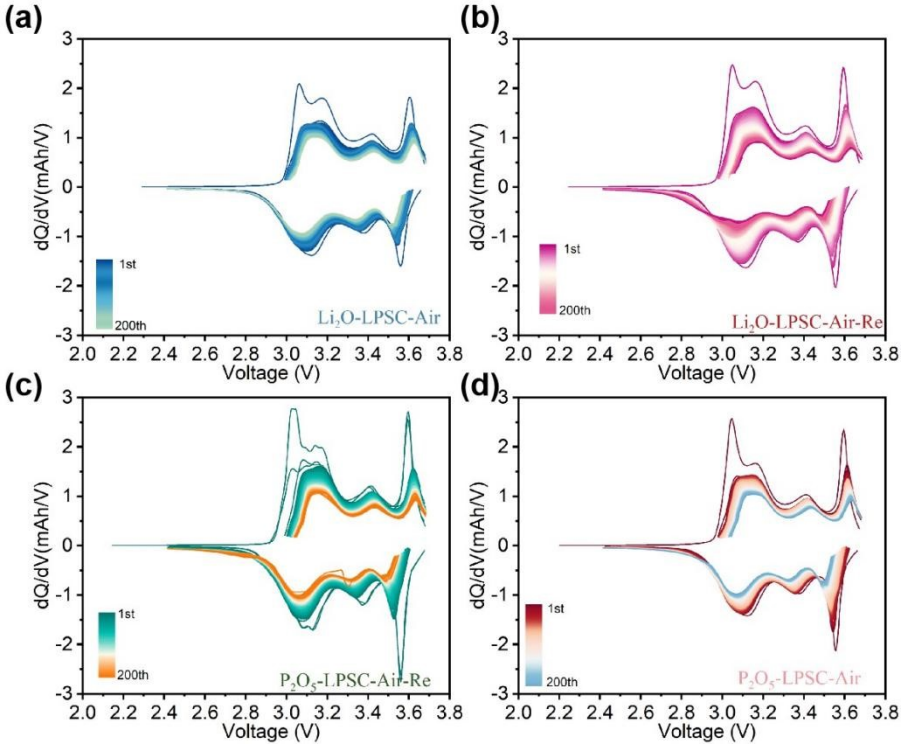

Fig. S14. The dQ/dV plots of above batteries: (a) ZrO_2@NCM/Li_2O-LPSC-Air/Li-In, (b) ZrO_2@NCM/Li_2O-LPSC-Air-Re/Li-In, (c) ZrO_2@NCM/P_2O_5-LPSC-Air/Li-In, and (d) ZrO_2@NCM/P_2O_5-LPSC-Air-Re/Li-In during long term cycling at 0.5C.

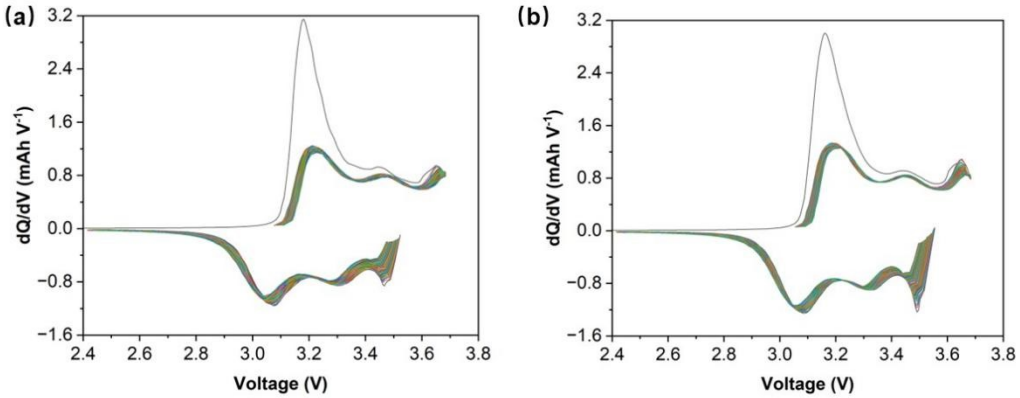

Fig. S15. The dQ/dV curves of ASSBs at various cycle numbers with (a) Li_2O-LPSC and (b) P_2O_5-LPSC electrolyte.

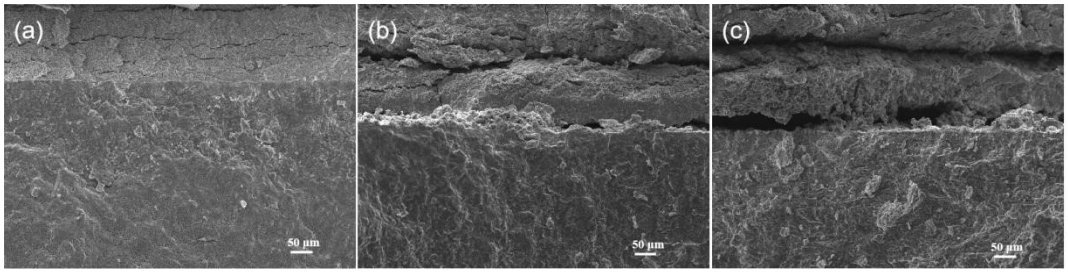

Fig. S16. Cross-sectional SEM images of the cathode/electrolyte interface. (a) Pristine interface before cycling. The interface after cycling in cells with (b) P_2O_5-LPSC and (c) Li_2O-LPSC as the sulfide electrolyte layer.

Table S1. Rietveld analyses for the XRD pattern of pristine-LPSC.

Space group F-43m, α = 9.823594 (Å), R_{wp} = 7.77%.

Atom site	Wykoff site	x	y	z	Occ.	U
Li1	16e	0.323000	0.024900	0.677000	0.5000	0.01
P1	4b	0.500000	0.500000	0.500000	1.0000	0.01
Cl1	4a	0.000000	0.000000	1.000000	0.6260	0.01
S1	4a	0.000000	0.000000	0.000000	0.3850	0.01
Cl2	4d	0.250000	0.250000	0.834000	0.8740	0.01
S2	4c	0.250000	0.250000	0.250000	0.6150	0.01
S3	16e	0.118800	-0.118800	0.618800	1.0000	0.01

Table S2. Rietveld analyses for the XRD pattern of Li_2O-LPSC.

Space group F-43m, α = 9.801222 (Å), R_{wp} = 6.81%.

Atom site	Wykoff site	x	y	z	Occ.	U
Li1	16e	0.323000	0.024900	-0.020100	0.4500	0.01
P1	4b	0.500000	0.500000	0.500000	1.0000	0.01
Cl1	4a	0.000000	0.000000	1.000000	0.6650	0.01
S1	4a	0.000000	0.000000	0.000000	0.3850	0.01
Cl2	4d	0.250000	0.250000	0.834000	0.8340	0.01
S2	4c	0.250000	0.250000	0.250000	0.1150	0.01
S3	16e	0.118800	-0.118800	0.618800	0.9250	0.01
O1	16e	0.118800	-0.118800	0.618800	0.0590	0.01
O1	4c	0.250000	0.250000	0.250000	0.0160	0.01

Table S3. Rietveld analyses for the XRD pattern of P_2O_5-LPSC.

Space group F-43m, α = 9.804764 (Å), R_{wp} = 9.70%.

Atom site	Wykoff site	x	y	z	Occ.	U
Li1	16e	0.262000	0.452200	-0.020100	0.4950	0.01
P1	4b	0.500000	0.500000	0.500000	1.0000	0.01
Cl1	4a	0.000000	0.000000	1.000000	0.6650	0.01
S1	4a	0.000000	0.000000	0.000000	0.3850	0.01
Cl2	4d	0.250000	0.250000	0.834000	0.8340	0.01
S2	4c	0.250000	0.250000	0.250000	0.1150	0.01
S3	16e	0.118800	-0.118800	0.618800	0.9250	0.01
O1	16e	0.118800	-0.118800	0.618800	0.0460	0.01

O1	4c	0.250000	0.250000	0.250000	0.0290	0.01

Table S4. Rietveld analyses for the XRD pattern of Li_2O-LPSC-Air.

Space group F-43m, α = 9.810267 (Å), R_{wp} = 9.72%.

Atom site	Wykoff site	x	y	z	Occ.	U
Li1	16e	0.317300	0.0317300	-0.020100	0.4560	0.01
P1	4b	0.500000	0.500000	0.500000	1.0000	0.01
Cl1	4a	0.000000	0.000000	1.000000	0.6650	0.01
S1	4a	0.000000	0.000000	0.000000	0.3850	0.01
Cl2	4d	0.250000	0.250000	0.834000	0.8340	0.01
S2	4c	0.250000	0.250000	0.250000	0.1130	0.01
S3	16e	0.118800	-0.118800	0.618800	0.9350	0.01
O1	16e	0.118800	-0.118800	0.618800	0.0610	0.01
O1	4c	0.250000	0.250000	0.250000	0.0140	0.01

Table S5. Rietveld analyses for the XRD pattern of Li_2O-LPSC-Air-Re.

Space group F-43m, α = 9.803784 (Å), R_{wp} = 9.34%.

Atom site	Wykoff site	x	y	z	Occ.	U
Li1	16e	0.317300	0.0317300	-0.020100	0.4560	0.01
P1	4b	0.500000	0.500000	0.500000	1.0000	0.01
Cl1	4a	0.000000	0.000000	1.000000	0.6650	0.01
S1	4a	0.000000	0.000000	0.000000	0.3850	0.01
Cl2	4d	0.250000	0.250000	0.834000	0.8340	0.01
S2	4c	0.250000	0.250000	0.250000	0.1220	0.01
S3	16e	0.118800	-0.118800	0.618800	0.9220	0.01
O1	16e	0.118800	-0.118800	0.618800	0.0610	0.01
O1	4c	0.250000	0.250000	0.250000	0.0140	0.01

Table S6. Rietveld analyses for the XRD pattern of P_2O_5-LPSC-Air.

Space group F-43m, α = 9.810349 (Å), R_{wp} = 9.29%.

Atom site	Wykoff site	x	y	z	Occ.	U
Li1	16e	0.317300	0.317300	-0.020100	0.4560	0.01
P1	4b	0.500000	0.500000	0.500000	1.0000	0.01
Cl1	4a	0.000000	0.000000	0.000000	0.6650	0.01
S1	4a	0.000000	0.000000	0.000000	0.4650	0.01

Cl2	4d	0.250000	0.250000	0.834000	0.8340	0.01
S2	4c	0.250000	0.250000	0.250000	0.5240	0.01
S3	16e	0.118800	-0.118800	0.618800	0.9450	0.01
O1	16e	0.118800	-0.118800	0.618800	0.0530	0.01
O1	4c	0.250000	0.250000	0.250000	0.0220	0.01

Table S7. Rietveld analyses for the XRD pattern of P_2O_5-LPSC-Air-Re.

Space group F-43m, α = 9.808733 (Å), R_{wp} = 10.39%.

Atom site	Wykoff site	x	y	z	Occ.	U
Li1	16e	0.31730	0.317300	-0.020100	0.4560	0.01
P1	4b	0.500000	0.500000	0.500000	1.0000	0.01
Cl1	4a	0.000000	0.000000	0.000000	0.6150	0.01
S1	4a	0.000000	0.000000	0.000000	0.3550	0.01
Cl2	4d	0.250000	0.250000	0.834000	0.8840	0.01
S2	4c	0.250000	0.250000	0.250000	0.1360	0.01
S3	16e	0.118800	-0.118800	0.618800	0.9350	0.01
O1	16e	0.118800	-0.118800	0.618800	0.0450	0.01
O1	4c	0.250000	0.250000	0.250000	0.0300	0.01

Table S8. Calculated total energy and average energy of an atom by DFT in (Li_2O or P_2O_5 doped $Li_{5.5}PS_{4.5}Cl_{1.5}$ in 4a and 16e sites within different structures.

Site	Structure	Total energy (eV)	Average energy /atom (eV)
16e	$Li_{22}P_4S_{18}Cl_6(Li_{5.5}PS_{4.5}Cl_{1.5})$	-212.90	-1.065
	$Li_{22}P_4S_{18}Cl_6O(Li_2O\text{-doping})$	-436.28	-2.181
	$Li_{22}P_4S_{18}Cl_6O(P_2O_5\text{-doping})$	-440.32	-2.202
4a	$Li_{22}P_4S_{18}Cl_6(Li_{5.5}PS_{4.5}Cl_{1.5})$	-209.28	-1.040
	$Li_{22}P_4S_{18}Cl_6O(Li_2O\text{-doping})$	-207.87	-1.039
	$Li_{22}P_4S_{18}Cl_6O(P_2O_5\text{-doping})$	-218.98	-1.095

Table S9. The detailed impedance values of each part of Li-In/LPSC/ZrO_2@Ni90 cells after rate tests.

Element	Parameter	Value (After cycle) rate performance			
		Li_2O-LPSC-Air	Li_2O-LPSC-Air-Re	P_2O_5-LPSC-Air	P_2O_5-LPSC-Air-Re
$R_{SE, bulk}/\Omega$	R	128 Ω	42.9 Ω	15.2Ω	39.2Ω
$R_{cathode/electrolyte}/\Omega$	R	142 Ω	44.3 Ω	63.6 Ω	35.3 Ω
	C_{eq}	25.3 nF	413nF	119nF	233nF
	α	697 m	719m	677m	281m
$R_{anode/electrolyte}/\Omega$	R	283.5 Ω	13.5 Ω	261 Ω	22 Ω
	C_{eq}	113 μF	560nF	198μF	123μF
	α	495 m	1021m	416m	641m
$R_{diffusion\ impedance}$	W	415DW	2.41 DW	103 DW	8.89 DW

Table S10. The detailed impedance values of each part of Li-In/LPSC/ZrO_2@Ni90 cells after cycling at 0.5C.

Element	Parameter	Value (After cycle) rate performance			
		Li_2O-LPSC-Air	Li_2O-LPSC-Air-Re	P_2O_5-LPSC-Air	P_2O_5-LPSC-Air-Re
$R_{SE, bulk}/\Omega$	R	110.8 Ω	124 Ω	69.5Ω	52.1Ω
$R_{cathode/electrolyte}/\Omega$	R	82.7 Ω	83.3 Ω	70 Ω	57.5 Ω
	C_{eq}	136 nF	134nF	257nF	211nF
	α	647 m	658m	490m	304m
$R_{anode/electrolyte}/\Omega$	R	445 Ω	290 Ω	265 Ω	237 Ω
	C_{eq}	87.9 μF	677nF	667μF	144μF
	α	513 m	541m	649m	526m

$R_{\text{diffusion impedance}}$	W	245DW	24.3 DW	9.01 DW	14 DW